Robust-Control-Based Design and Comparison of an Adaptive Controller for the VEGA Launcher

Diego Navarro-Tapia* and Andrés Marcos †

Technology for Aerospace Control (TASC) Lab.,

Department of Aerospace Engineering, University of Bristol, Bristol, BS8 1TR, United Kingdom

Samir Bennani‡

European Space Agency, ESTEC, Noordwijk, 2201AZ, The Netherlands

Christophe Roux§

AVIO, VEGA GNC Department, Colleferro, 00034, Italy

This article presents the design and evaluation of an adaptive controller for the atmospheric phase VEGA launcher. This design uses an Adaptive Augmenting Control (AAC) architecture to further extend the performance and capabilities of a robust-control structured $\mathcal{H}_\infty$ controller, which was designed based on the current VEGA control architecture. The main goal of this paper is first, to explore adaptive features for the VEGA control system and second, to evaluate its performance and robustness properties. To that end, the adaptive controller is compared with the structured $\mathcal{H}_\infty$ baseline controller and a linear parameter varying (LPV) design (both without adaptive augmentation). The three controllers are analysed for several extreme off-nominal condition tests using a high-fidelity, nonlinear simulator of the VEGA launcher. And the main performance indicators for the atmospheric phase are evaluated through a Monte-Carlo campaign. The results show that the adaptive and LPV controllers successfully provide stability under extreme adverse flight conditions over the non-adaptive robust controller. It is also shown that the LPV approach provides a more formal and methodological way to achieve these improvements.

I. Introduction

The flight control system of a launch vehicle is heavily impacted in atmospheric phase by several undesired effects such as structural loads (coming from wind gusts), aerodynamic instability (due to vehicle's design aspects), parameter dispersions, coupling between the rigid-body and the elastic behaviour of the vehicle, and nonlinearities in the actuators. All these factors make the design of the atmospheric-phase control system of a launch vehicle a difficult task.

The new European small launch vehicle, VEGA, uses a classical design approach for the Thrust Vector Control (TVC) system consisting in proportional-derivative rigid-body gains plus bending filters.[1] This design approach has demonstrated, via thirteen consecutive successful flights, that the current VEGA control laws are able to cope with very tight industrial requirements. Nonetheless, it is recognized that it is hard to achieve stability and performance robustness characteristics along the atmospheric phase and that this strategy results in a very time-consuming design, tuning and validation process.

*PhD researcher, Department of Aerospace Engineering, University Walk. Student AIAA member

†Senior Lecturer, Department of Aerospace Engineering, University Walk. Senior AIAA member.

‡GNC launcher system expert, ESA-ESTEC GNC Section, Keplerlaan 1. Senior AIAA member.

§VEGA Control Engineer, VEGA GNC Department, via Latina. Senior AIAA member.

Therefore, considering the competitiveness of the launch service market, control system improvements such adaptive control features and more methodological synthesis techniques must be proposed. In this scenario, robust control synthesis techniques such as the structured $\mathcal{H}_\infty$ and linear parameter varying (LPV) techniques have been explored for the VEGA launcher in references.[2–4] It is shown that these two robust control techniques can be used to improve the performance and robustness of the system while providing a more systematic design process approach with respect to the traditional state-of-practice, as well as, a reduced tuning and design effort required for each mission. In addition, the control design techniques used are well connected with robust analysis techniques such as the structured singular value μ, which help to facilitate analytically assessing the guaranteed bounds on robust stability and performance.[5]

Despite the above advantages, there is a push in the launcher community and industry, to study and develop adaptive controllers. Thus, in this paper, the adaptive control architecture used by NASA's Space Launch System[6] (SLS) is applied to the VEGA launcher. The SLS flight control system relies on a baseline (typically classical) controller which is augmented by an adaptive control law. This adaptive augmenting control provides minimal adaptation under nominal conditions, improves robustness to launch vehicle failures and provides extended safety envelope capabilities.[6–8] This adaptive strategy has successfully been demonstrated in flight tests on a F/A-18 aircraft.[9] Nevertheless, due to the adaptive behaviour of the system and to the nonlinear characteristics of the adaptive control law, there are not formal techniques to apply the classical linear stability margins used by industry to verify and validate the designs. This topic has raised the attention of the control research community in recent years. Most of the works looking at this important issue rely on simulation-based nonlinear stability techniques.[10–12]

This article aims first to explore adaptive control features for the VEGA control system to augment a robust-control structured $\mathcal{H}_\infty$ controller and second, to compare the performance and robustness of this robust-based adaptive controller with a full-order LPV design.

The layout of this paper is as follows: Section II briefly describes the VEGA launch vehicle, mission and nonlinear simulator. This section also presents the structured $\mathcal{H}_\infty$ controller that will be used as baseline for the adaptive augmentation, and the LPV controller that will serve to benchmark the latter. Section III describes the adaptive augmentation control architecture and the description of the adaptive control law tuning. Then in Section IV, the three controllers presented in this paper are evaluated and compared using extreme off-nominal, nonlinear, time-domain simulations and also via Monte-Carlo simulations. Finally, Section V ends with the conclusions.

II. Robust Control Design for the VEGA launcher

A. VEGA launcher and mission

VEGA launcher is the new European Small Launch Vehicle developed under the responsibility of the European Space Agency (ESA) and European Launch Vehicle (AVIO S.p.A.) as prime contractor. The launcher has successfully performed thirteen launches since its maiden flight on 13th February 2012.

VEGA is a single-body launcher, which follows a four stage approach (see Figure 1) formed by three solid propellant motors (P80, Zefiro 23 and Zefiro 9) providing thrust for the first three stages; and, a bi-propellant liquid engine on the 4th stage (AVUM). All stages are controlled using a TVC. There is also a Roll and Attitude Control System (RACS) performing 3-axes control during the ballistic phase and roll rate control during the propelled phases.

The VEGA launcher performs a wide range of missions with specific configurations and trajectories. In this work, all the simulations and designs are applied to the actual VEGA mission data[13] . The payload of this mission was the Sentinel-2A satellite, part of Europe's Copernicus Earth observation program. Figure 2 shows the nominal flight responses for altitude, Mach and dynamic pressure for the atmospheric phase. It can be seen that during this first phase, the launch vehicle reaches Mach 5 and approximately 50 km of altitude.

B. VEGA high-fidelity nonlinear simulator

The high-fidelity, nonlinear 6 degrees-of-freedom (DOF) simulator used in this work is called VEGACONTROL.[14] This simulator is tailored to simulate the atmospheric phase for the VEGA program and is prepared for accelerated-time simulations (through protected and compiled code). In previous work,[14] this simulator was compared to that used by ELV for final validation of their VEGA control

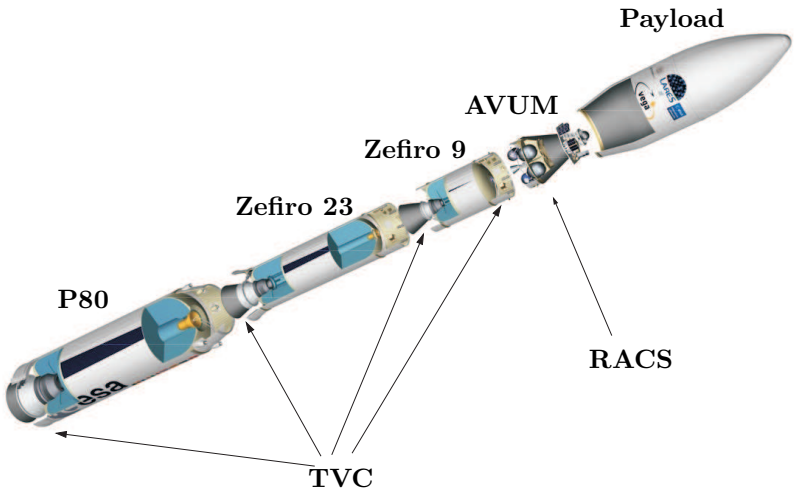

Figure 1. VEGA launcher stage configuration

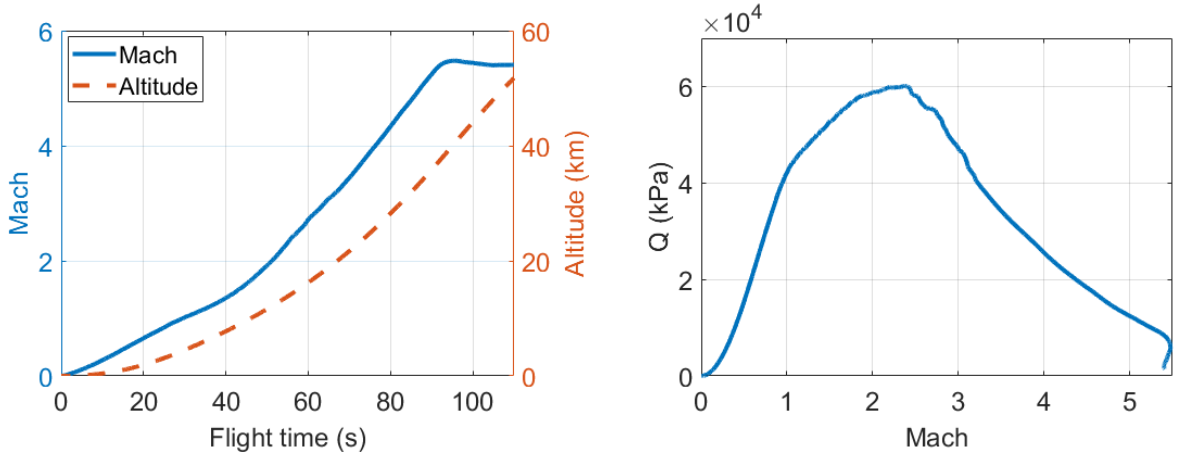

(a) Mach and altitude versus time

(b) Dynamic pressure versus Mach

Figure 2. Atmospheric-phase VEGA VV05 mission parameters

designs, and was found to be highly representative for the atmospheric phase. VEGACONTROL allows to scatter more than 125 different operational parameters by means of normalised flags including mass-center-inertia parameters, aerodynamics, wind profiles, inertial navigation system (INS) mounting and thrust parameters among others. The high-level architecture of this simulator is composed of four main model blocks, as it can be seen in Figure 3.

The launch vehicle (LV) model contains the 6 DOF motion of the vehicle, which includes:

- 6 DOF rigid-body model, accounting for the rotational and translational dynamics of the vehicle;
- Elastic and sloshing modes;
- Tail-wag-dog (TWD) model, including the inertia forces and moments created by the motion of the gimbaled engines;
- Full external environment (rotating Earth, atmosphere and wind);
- Nonlinear aerodynamics (including aero-elastic effects);
- Disturbances (bias, offsets).

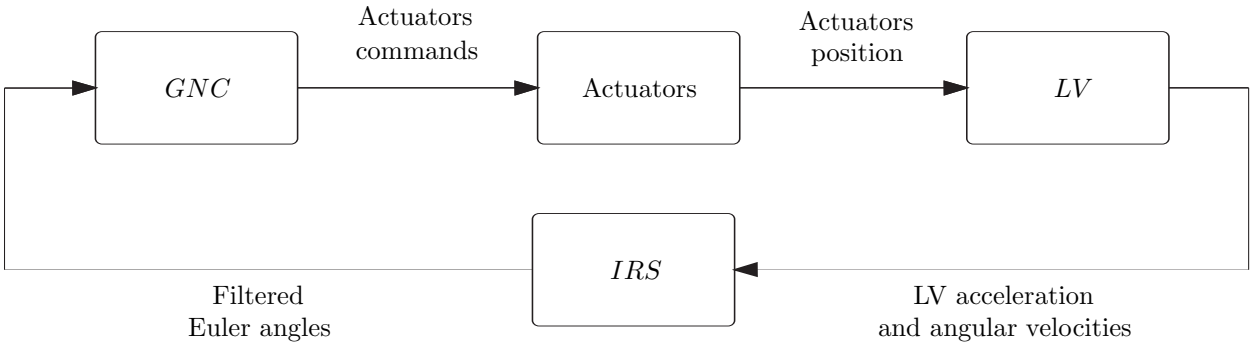

Figure 3. Simplified scheme of the VEGA atmospheric phase high-fidelity nonlinear simulator

The inertial reference system (IRS) includes a detailed model of the INS (calibration and mounting errors, quantization and noise on measured velocity and angles) while the guidance, navigation and control (GNC) model comprises a full representative code implementing the VEGA GNC and flight management (FM) algorithms.[1] This block uses the measurements from the INS to compute the necessary nozzle deflections to follow the attitude commands from the guidance function. Finally, these actuator commands are delivered to two orthogonal nozzle electro-mechanical actuators (EMA). The actuators block incorporates a detailed model of the nonlinear TVC actuators (with saturations in deflection and rate, backlash, delays and bias) and also of the roll and attitude control system (RACS) with thermal and thrust dynamics.

C. Structured $\mathcal{H}_\infty$ design

This controller was designed using the structured $\mathcal{H}_\infty$ synthesis technique.[15,16] This technique allows using the $\mathcal{H}_\infty$ robust control design optimization while specifying the structure of the controller.

For this design, the rigid-body controller and bending filters were parametrized and then optimized simultaneously. This joint design simplifies the synthesis process and reduces the tuning effort prior to each mission. It is important to remark that this design was performed taking parametric uncertainties into account as well as including a wind disturbance model. The detailed synthesis process of this controller is provided in reference.[3]

The TVC structure of the design can be seen in Figure 4a. The rigid-body controller is composed of 4 gains (a proportional-derivative (PD) controller for the attitude and drift channels) and a pseudo-derivative filter $H_2(s)$ which computes the attitude error signal ψ_e. In addition, a bending filter $H_3(s)$, which notches the first bending mode and attenuates the upper modes, is also included in the architecture. The final controller has 15 states and the rigid-body gains and the bending filter $H_3(s)$ parameters are gain-scheduled using the non-gravitational velocity (VNG) as a scheduling parameter.

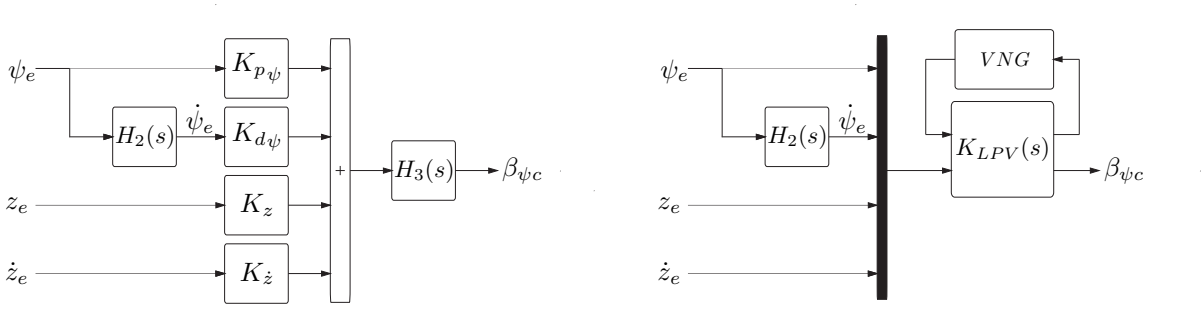

(a) Structured $\mathcal{H}_\infty$ design TVC structure

(b) LPV design TVC structure

Figure 4. TVC structures for the VEGA robust control designs

D. Linear Parameter Varying (LPV) design

This controller was designed using the LPV synthesis technique. This design approach allows taking into account the varying behaviour of the system as captured by a measured parameter. In particular, this design was performed using VNG as the scheduling parameter, with a known rate bound defined by the non-gravitational acceleration. Note that VNG is the actual VEGA scheduling variable.[1] The reader is referred to reference[4] for further details about the synthesis process.

The TVC structure of this design is shown in Figure 4b. This controller is composed of a full-order controller, which includes the rigid-body controller and bending filters functionalities, and the pseudo-derivative filter $H_2(s)$. In total, this design has 23 states and is implemented using a Simulink block provided in the LPVTools toolbox.[17] Note that this block performs a multidimensional linear interpolation to evaluate the state-space matrices of the controller at the specified parameter vector.

III. Adaptive Augmentation Control for the VEGA launcher

In this section, the VEGA launcher control architecture presented in Section II.C is augmented to explore adaptive features. First, the adaptive control scheme employed in this work is described and then its tuning is presented.

A. Adaptive augmenting control structure

As mentioned before, the adaptive control strategy used in this article is based on the NASA's Space Launch System (SLS) presented in reference[7] (see Figure 5). It should be noted that the SLS algorithm has evolved and there are currently more modern versions of the adaptive control law.[8] Nonetheless, the adaptive architecture presented here still represents a good benchmark scenario to study adaptive augmentation control functionalities.

The adaptive augmentation relies on a baseline controller, which is designed to operate under nominal conditions. This baseline controller is then augmented by an adaptive control law which has the following main objectives: 1) adapt minimally in nominal conditions; 2) increase performance and command tracking in dispersed conditions and when disturbances produce large errors; 3) prevent loss of vehicle (LoV) in extreme off nominal conditions.

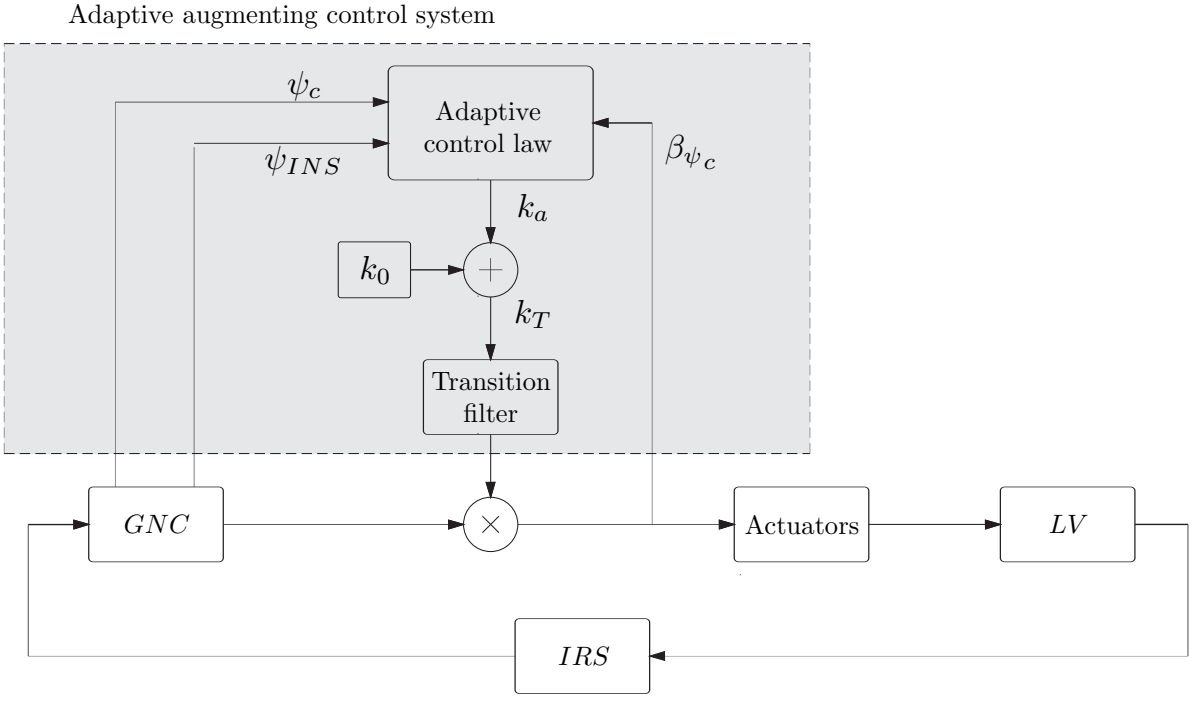

Figure 5. Nonlinear simulator with adaptive augmentation

The SLS adaptive augmenting control system is based on a multiplicative law. As it can be seen in Figure 5, the actual actuators commands are computed by multiplying the controller output by the total loop gain k_T, which is defined in equation 1. This gain is composed of two terms: a fixed gain k_0, which establishes a lower bound for k_T and the adaptive gain k_a, which is the output of the adaptive control law block.

$$\underbrace{k_T}_{\text{Total loop gain}} = \underbrace{k_0}_{\text{Minimum total loop gain}} + \underbrace{k_a}_{\text{Adaptive gain}} \tag{1}$$

Since under nominal conditions the adaptive action should be minimal then $k_T \approx 1$. On the other hand, under dispersed conditions, k_T will increase or decrease the loop gain according to the adaptive control law.

The allowable values for k_T are defined based on the nominal stability gain margins of the system. For instance, assuming a nominal low-frequency gain margin of 6 dB, the lower bound for k_T is defined as $k_{Tmin} = k_0 = 0.5$. For the maximum allowable k_T, the high-frequency gain margin is considered (i.e. a high-frequency gain margin of -6 dB corresponds to a magnitude of 2). Since k_0 is a fixed gain, this upper limit for k_T defines in turn a maximum adaptive gain (if $k_{Tmin} = 2$, then $k_{amax} = 1.5$).

The total loop gain k_T is then passed through a transition filter (see Figure 5). This filter activates the adaptive action at t=15s to avoid the vertical flight phase and the start of the pitch over (thus, $k_T = 1$ for $t < 15s$). Furthermore, to minimise transients when activation, a 2^{nd} order transition filter interpolates the initial value $k_T = 1$ and the output of the adaptive augmentation.

Finally, the adaptive control law defines the rate dynamics of the adaptive gain k_a given by the following first-order ordinary differential equation:

$$\dot{k}_a = \underbrace{H^e_{LP} k_e {e_r}^2}_{\text{Adaptive error}} - \underbrace{\frac{k_a}{k_{amax}} H^e_{LP} k_e {e_r}^2}_{\text{Logistic damper}} - \underbrace{k_{sd} k_a y_s}_{\text{Spectral damper}} - \underbrace{k_\beta (k_T - 1)}_{\text{Leakage}} \tag{2}$$

Equation 2 is formalised using the initial condition $k_a(0) = 0.5$ to properly initialize the adaptive augmentation control system ($k_T(0) = 1$). Also note that the same adaptive control law is employed for pitch and yaw axes under the assumption that they are decoupled. It should be remarked that there are three main differences between the adaptive control law presented in this work and the one described in reference.[7] The first one is the transition filter, which alleviates the transients when the adaptive augmentation is activated. The second novelty is the use of the filter H^e_{LP} to smooth the output of the adaptive error and the logistic terms. And third, and very critical to correctly compare with the results from that reference, is that in here the baseline controller is robust and gain scheduled while in reference[7] it is a single LTI controller.

Next, the different terms of equation 2 are explained in detail.

1. Adaptive error

The adaptive error term increases the adaptive gain driven by the reference model error e_r, which is defined as $e_r = \psi_{INS} - \hat{\psi}_{INS}$. The estimated attitude angle $\hat{\psi}_{INS}$ is computed using the second order linear parameter varying (LPV) reference model shown in equation 3. This LPV model uses also the non-gravitational velocity (VNG) as scheduling parameter ρ.

$$\hat{\psi}_{INS}(s, \rho) = \frac{2\zeta_r(\rho)\omega_r(\rho)s + {\omega_r}^2(\rho)}{s^2 + 2\zeta_r(\rho)\omega_r(\rho)s + {\omega_r}^2(\rho)} \psi_c \tag{3}$$

where $\zeta_r(\rho)$ and $\omega_r(\rho)$ are chosen to approximate the linear closed-loop dynamics at every grid point along the ascent trajectory.

The signal error e_r is multiplied by the adaptive error gain k_e, which is tuned to achieve minimal adaptation for the nominal flight. The scaled adaptive error signal is passed through a low-pass filter H^e_{LP} to avoid high-frequency fluctuations on the adaptive gain.

2. Logistic damper

The logistic damper term is computed by scaling the adaptive error term by a ratio between the adaptive gain k_a and its maximum value k_{amax}. Using this configuration, the gain loop is decreased as k_a approaches its maximum value k_{amax}. Therefore, the logistic damper imposes an upper bound for the adaptive gain k_a defined by k_{amax}.

3. Spectral damper

The spectral damper term reduces the adaptive gain to suppress the effect of undesired high-frequency dynamics in the actuators commands. This term is based on the spectral damper signal y_s which is computed as follows:

$$\begin{aligned} y_{HP} &= H^{sd}_{HP}\beta_{\psi_c} \\ y_s &= H^{sd}_{LP}(y_{HP})^2 \end{aligned} \tag{4}$$

The actual actuator command β_{ψ_c} is filtered through a high-pass (HP) filter H^{sd}_{HP}, which captures undesired dynamics at frequencies higher than the rigid-body dynamics of the launch vehicle. This filtered signal y_{HP} is then squared and smoothed through another low-pass (LP) filter H^{sd}_{LP}. This filter removes high-frequency fluctuations on y_s and thus on the total loop gain k_T.

Finally, the spectral damper signal y_s is multiplied by the adaptive gain k_a as well as the spectral damping gain k_{sd}, which is also tuned to achieve minimal adaptation for a nominal flight.

4. Leakage

The leakage term is a compensation model which attempts to lead k_T towards unity. This term is tuned through a leakage gain k_β, which is tuned to achieve minimal adaptation in a nominal test case.

B. Adaptive control law tuning

The adaptive control law was tuned using as baseline (i.e. nominal-conditions active) controller the structured $\mathcal{H}_\infty$ design presented in Section II.C. A summary of the tuned parameters is shown in Table 1.

Table 1. Adaptive augmentation parameters

Gain	Value
k_0	0.5
k_{amax}	1.5
k_e	200
k_{sd}	5000
k_β	0.25

For the tuning process the upper and lower limits of the total loop gain k_T are determined first. As mentioned before, these bounds are chosen based on the nominal stability gain margins of the system (without adaptation). The baseline controller globally achieves ±6 dB nominal rigid-body margins along the atmospheric phase. Thus, to preserve the robustness characteristics of the baseline system, $k_{Tmin} = 0.5$ and $k_{Tmax} = 2$. This results in the following gains: $k_0 = 0.5$ and $k_{amax} = 1.5$.

The other gains of equation 2 (k_e, k_{sd} and k_β) are tuned manually based on nonlinear simulations. The values shown in Table 1 were obtained to achieve minimal adaptation in a nominal test case. No other test cases were considered for the tuning to avoid tailoring the design for a specific mission scenario.

Similarly, the filters in the adaptive control law are also tuned manually. Figure 6 shows the Bode plots of the adaptive error and spectral damper filters. The adaptive error filter H^e_{LP} is a second-order low-pass filter which is tuned to smooth and remove the high-frequency components of the adaptive error signal e_r. The spectral damper filters are also second-order filters (see Figure 6b). H^{sd}_{HP} is designed to capture high-frequency components above the rigid-body bandwidth, while H^{sd}_{HP} is also tuned to smooth the spectral damper signal y_s. Note that all those filters are discretized for the final implementation in the nonlinear, high-fidelity simulator.

Unlike reference[7] where the adaptive controller was only tested for the pitch axis, in this work the adaptive augmentation is implemented in both axes, pitch and yaw. Note that the VEGA control system only limits the roll axis dynamics during the atmospheric phase. During this phase, the RACS only performs roll control if the roll rate is over a certain threshold.

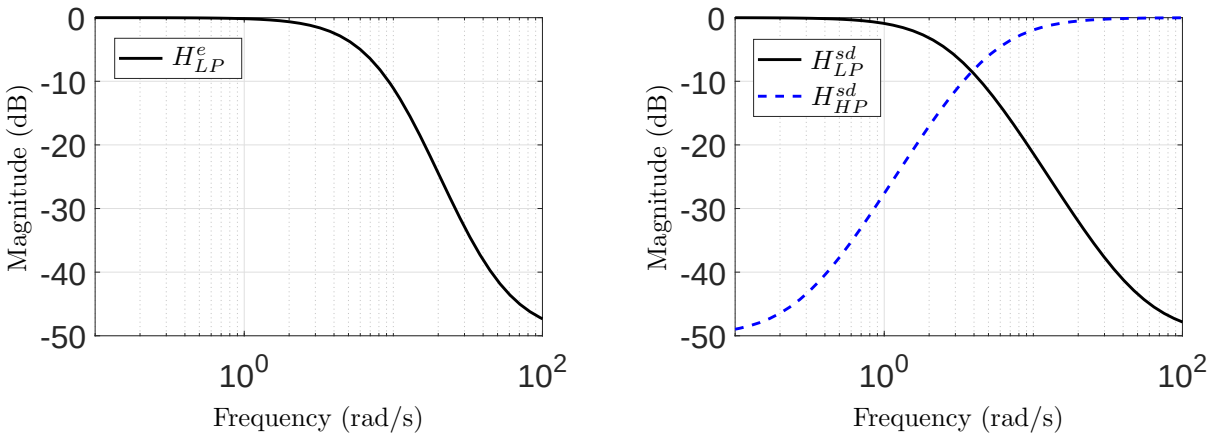

(a) Adaptive error filter

(b) Spectral damper filters

Figure 6. Bode plots of the adaptive control law filters

IV. Simulation Results

This section analyses and compares the performance and robustness of the controllers presented in Sections II.C, II.D and III.B. These three controllers are evaluated using a specific set of nonlinear, time-domain simulations and also via Monte-Carlo simulations.

A. Nonlinear test cases

To evaluate the performance of the adaptive controller with respect to the non-adapted (i.e. baseline) structured $\mathcal{H}_\infty$ and the LPV design, a set of nonlinear test cases are selected to benchmark and stress the designs. In this work, the following 4 test cases are considered:

- ***Test case 1****: nominal VV05 flight*
Objective: verify that the adaptive augmentation provides minimal adaptation under nominal conditions (those encountered during the selected mission, i.e. VV05).

- ***Test case 2****: nominal VV05 flight + VV05 wind*
Objective: study the effect of wind disturbance on the adaptive controller (using the real mission wind profile).

- ***Test case 3****: dispersed VV05 flight + VV05 wind (all uncertainties ± 100%)*
Objective: analyse the effect of the adaptation at the limits of the mission uncertainty range. Two vertex combinations are used: all uncertainties at 100% and at -100%.

- ***Test case 4****: dispersed VV05 flight + VV05 wind (all uncertainties beyond operation range)*
Objective: explore the extended safety envelope capabilities that the adaptive scheme can provide by increasing the level of uncertainties beyond the operation range of the mission.

Due to space concerns, only two of the previous test cases are explained in detail.

1. ***Test case 1**: nominal VV05 flight*

This test case aims to verify that the contribution from the adaptive augmentation is very small under nominal conditions. For this simulation, all VEGACONTROL flags are set to 0 and the wind disturbance is disabled.

Figure 7 shows the total loop gain k_T for the pitch (plot 7a) and yaw axis (plot 7b). It can be seen that $k_T \approx 1$ for both axes along the atmospheric phase. Therefore, since the adaptive action is minimal, the launch vehicle is essentially controlled by the structured $\mathcal{H}_\infty$ baseline controller.

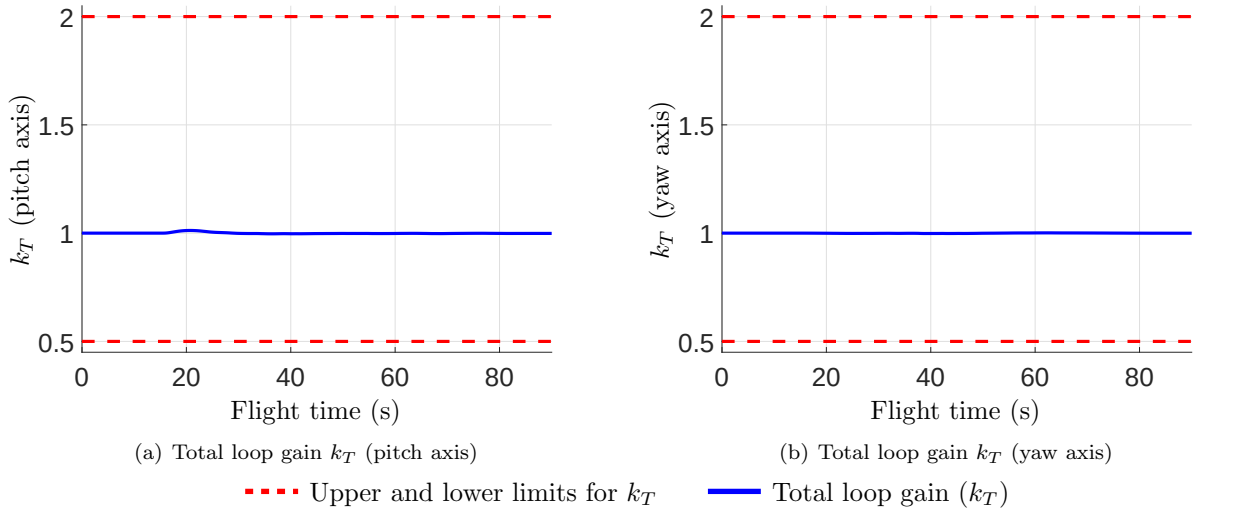

(a) Total loop gain k_T (pitch axis)

(b) Total loop gain k_T (yaw axis)

Figure 7. Total loop gain k_T analysis for nominal test case

The dynamics of the adaptive control law and the contribution of each of its terms (see equation 2) can be analysed in Figure 8. Unlike for the yaw axis (plot 8b), the rate of the adaptive gain in the pitch axis (plot 8a) presents a transient when the adaptive augmentation is activated at t=15s. The reason is that the launch vehicle is still following the pitch over manoeuvre and that creates an initial adaptive error contribution, which is rapidly counteracted by the leakage term to have $k_{\dot{a}} \approx 0$.

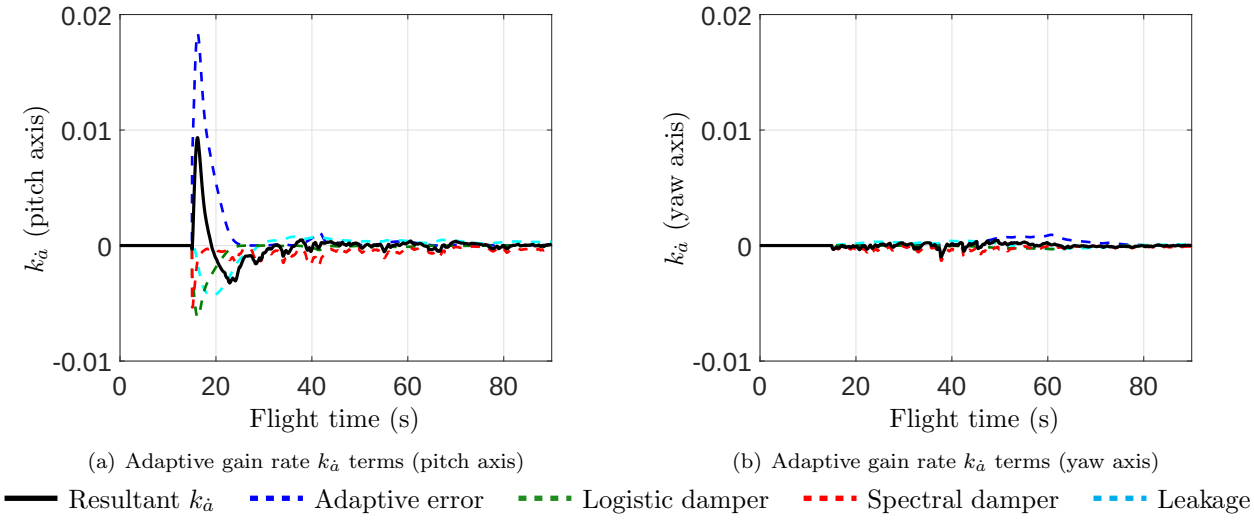

(a) Adaptive gain rate $k_{\dot{a}}$ terms (pitch axis)

(b) Adaptive gain rate $k_{\dot{a}}$ terms (yaw axis)

Figure 8. Adaptive rate gain $k_{\dot{a}}$ analysis for nominal test case

2. ***Test case 4****: dispersed VV05 flight + VV05 wind (all uncertainties beyond operation range)*

In this test, the level of uncertainties is increased until a major failure such as instability or loss of vehicle is observed. For this configuration, a severe launch vehicle failure is identified when all the flags are set to 1.35 (135% level of uncertainty). In particular, the structured $\mathcal{H}_\infty$ baseline controller becomes unstable during the maximum dynamic pressure region (t=50-60s) causing a loss of vehicle at t=60s. This failure event can be seen in Figure 9, where the flight responses of three key performance metrics such as attitude errors, gimbaled commands and structural loads are shown.

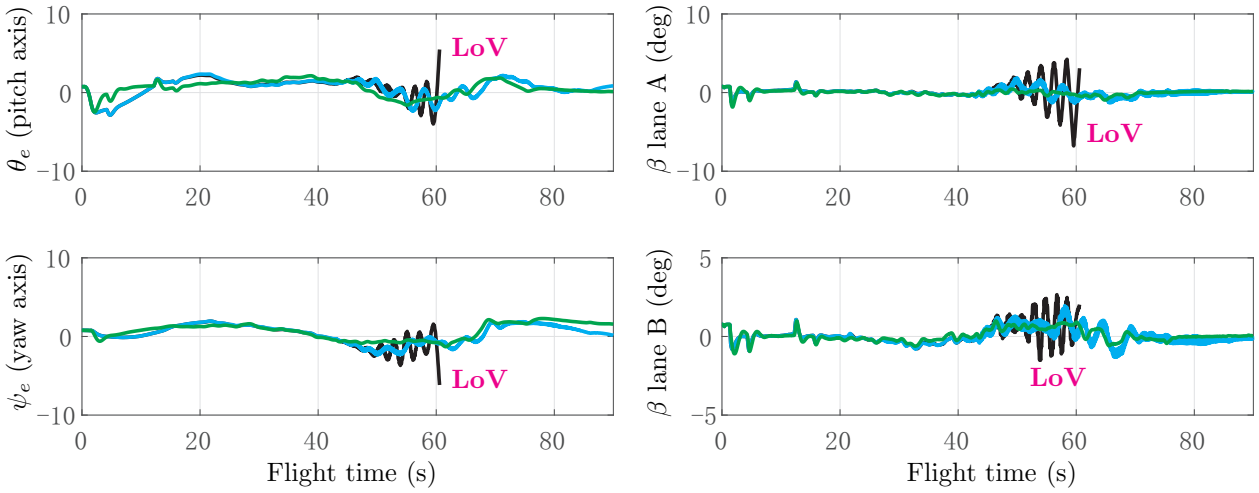

(a) Attitude errors

(b) Actuator commands

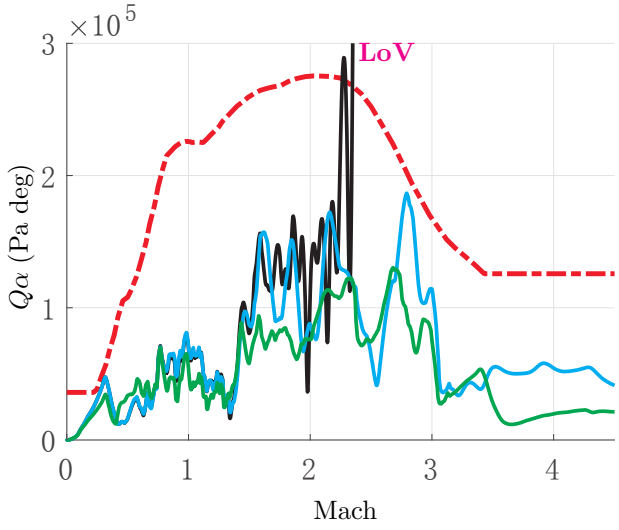

(c) Load requirement Qα

Figure 9. Nonlinear dispersed flight responses (uncertainties 135%)

On the other hand, the adaptive structured $\mathcal{H}_\infty$ controller manages to control the instability and prevents the loss of vehicle. To understand this behaviour, the total loop gain k_T and the rate of the adaptive gain $k_{\dot{a}}$ are shown in Figure 10 and 11. It is interesting to observe that the adaptive control law detects high-frequency action in the actuation channel and reduces the adaptive gain to maintain the stability. This mechanism is mainly activated by the spectral damper term at t=45s (see Figure 11), which produces a sudden reduction of the total loop gain (see Figure 10).

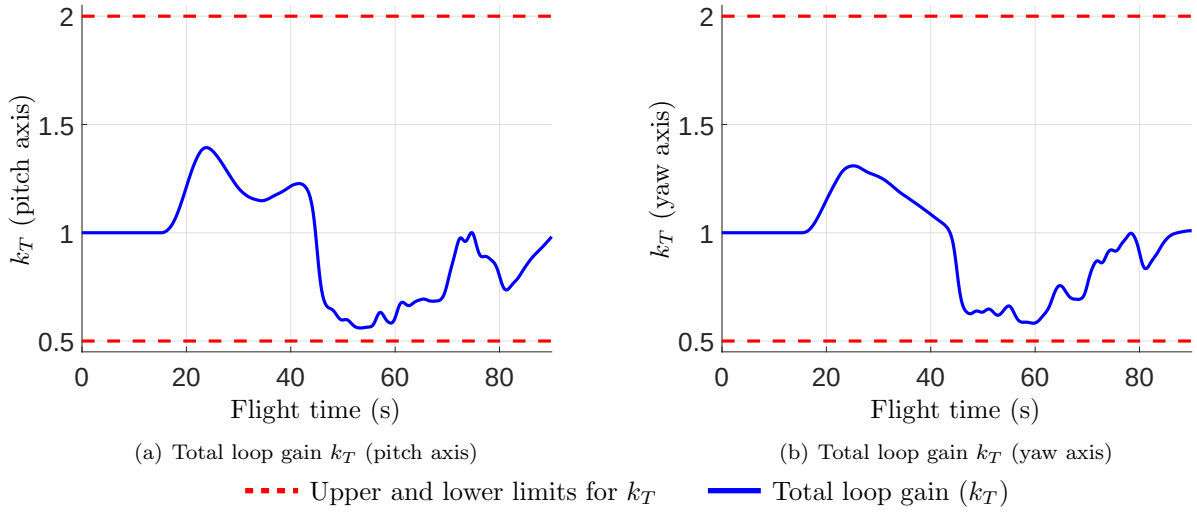

(a) Total loop gain k_T (pitch axis)

(b) Total loop gain k_T (yaw axis)

Figure 10. Total loop gain k_T analysis for dispersed test case (uncertainties 135%)

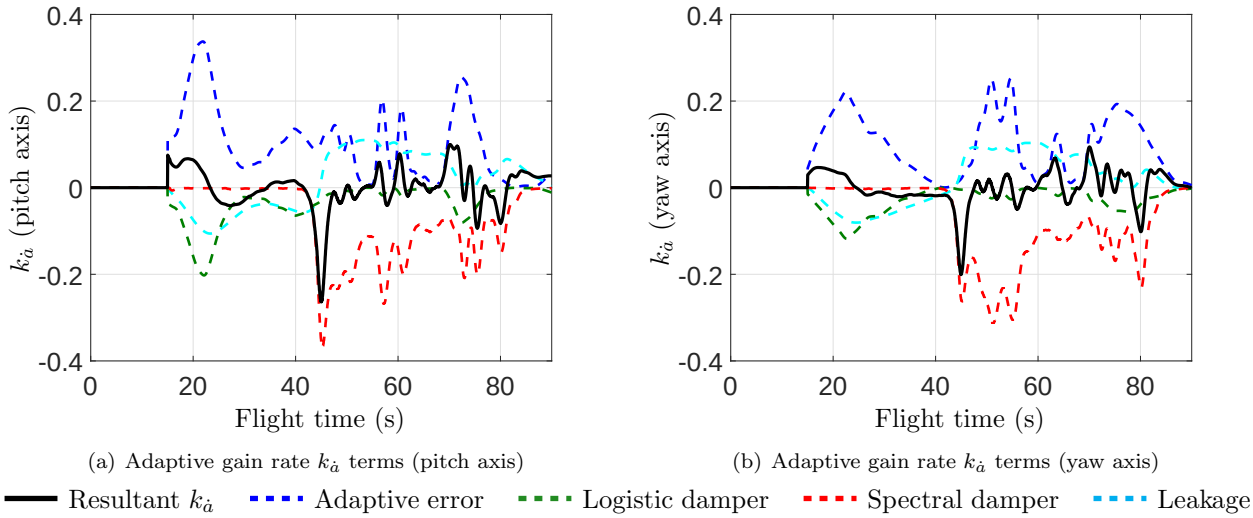

(a) Adaptive gain rate $k_{\dot{a}}$ terms (pitch axis)

(b) Adaptive gain rate $k_{\dot{a}}$ terms (yaw axis)

Figure 11. Adaptive rate gain $k_{\dot{a}}$ analysis dispersed test case (uncertainties 135%)

Finally, it is worthy noting that the LPV controller also manages to prevent the loss of vehicle under such extreme flight conditions. Indeed, it is observed that the LPV controller improves the overall performance with respect to the adaptive controller. It significantly reduces the $Q\alpha$ peak at Mach 2.8 (see plot 9c) and although less noticeable the LPV controller actuation channel does not show high-frequency components (plot 9b).

B. Monte-Carlo campaign

To evaluate the performance and robustness, a Monte-Carlo (MC) campaign of 500 runs is performed (the same MC set-up is applied to the three controllers. For each run, the same nominal VEGA VV05 flight trajectory is used but the operational parameters are all dispersed randomly. It should be remarked that the uncertainty range of the mission has been increased by 30% from their standard range to analyse the controllers under more perturbed flight conditions. Also note that the measured wind from the VEGA VV05 mission is also used in this MC analysis.

Figure 12 shows the 500 MC time-domain responses of the gimbaled commands for the three controllers. In darker lines, the corresponding simulations using the VEGA VV05 mission nominal dispersions are shown for each controller to serve as reference. It is observed that there are some critical launch vehicle failures for the structured $\mathcal{H}_\infty$ baseline controller, while the adaptive and LPV controllers manage to prevent the loss of vehicle. These failure cases are caused by a significant reduction ($\approx 26\%$) on the nominal first bending mode frequency. This causes interactions between the rigid-body and the bending modes leading to instability.

The results confirm the behaviour shown in Section IV.A. That is, the adaptive augmentation is able to prevent a major launch vehicle failure under extreme off-nominal conditions while the LPV controller shows also good robustness characteristics against very high dispersions.

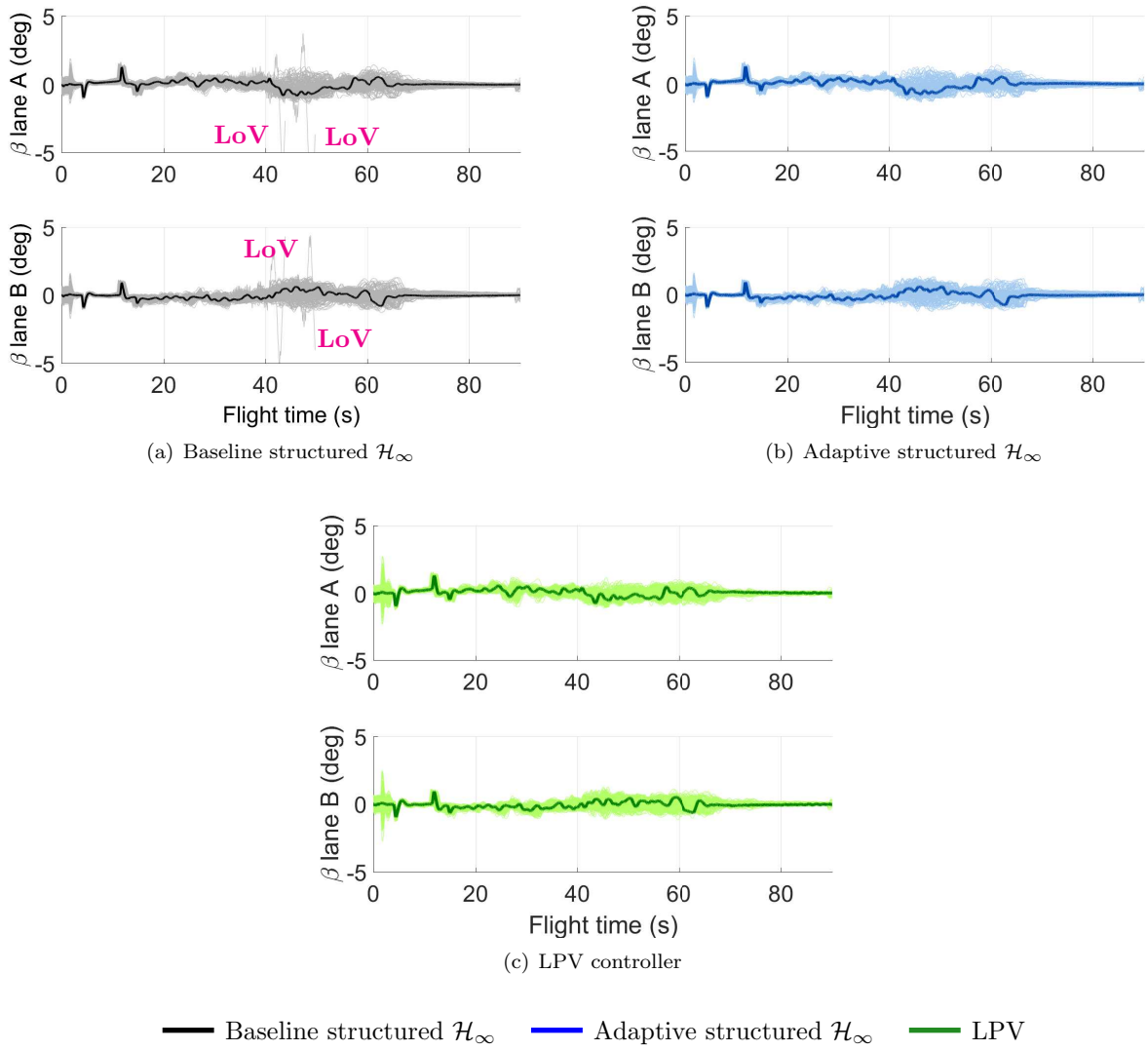

(a) Baseline structured $\mathcal{H}_\infty$

(b) Adaptive structured $\mathcal{H}_\infty$

(c) LPV controller

Figure 12. Extended Monte-Carlo (uncertainty range 130%) TVC actuator command responses

The same conclusions can be extracted looking at Figure 13, where the aerodynamic load performance indicator $Q\alpha$ is shown for the three controllers. The adaptive augmentation manages to keep the structural loads under the $Q\alpha$ safety envelope for all the cases. In addition, it can be seen that the LPV controller not only achieves this but also reduces noticeably the aerodynamic loads with respect to the other two cases.

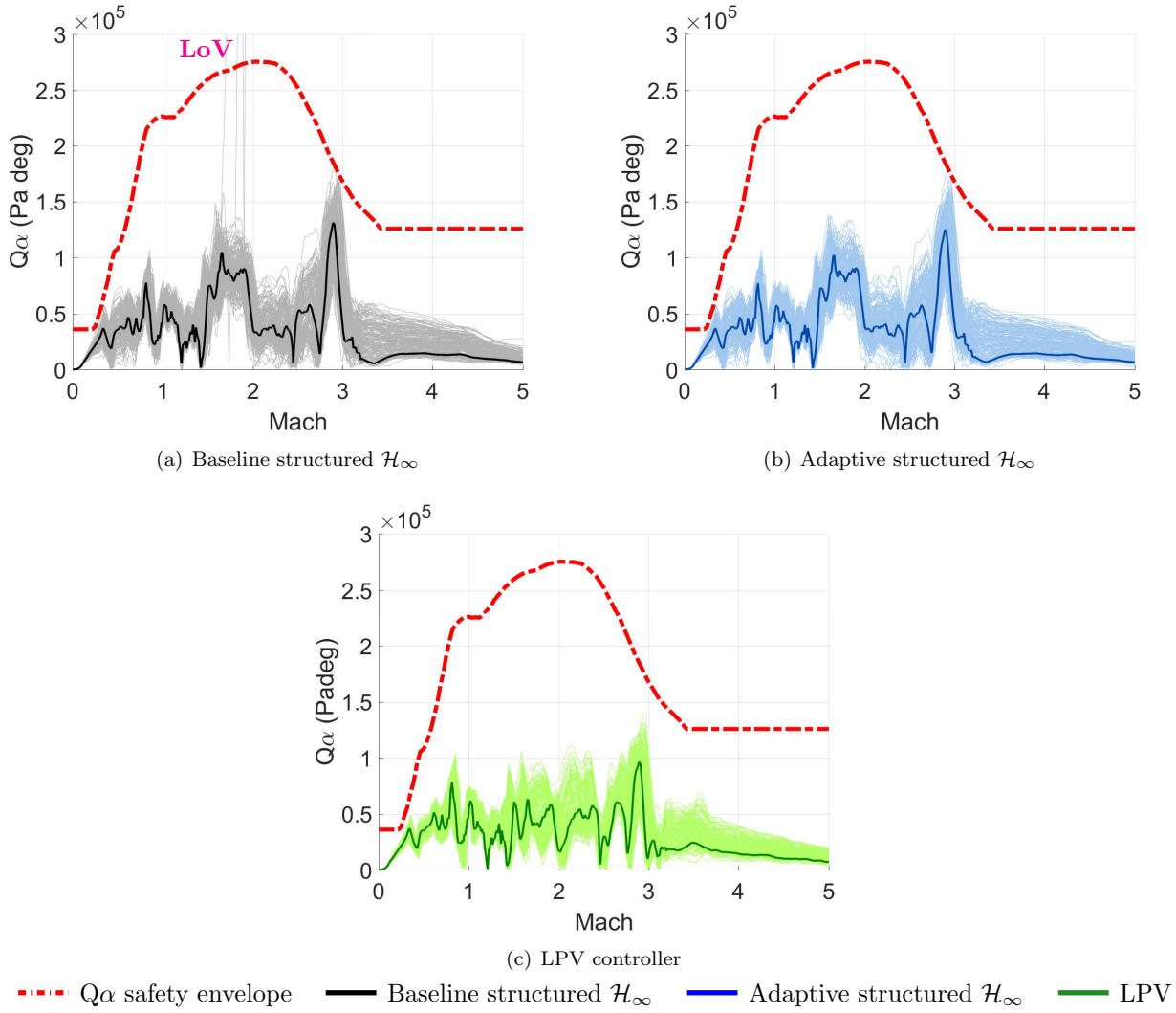

(a) Baseline structured $\mathcal{H}_\infty$

(b) Adaptive structured $\mathcal{H}_\infty$

(c) LPV controller

Figure 13. Extended Monte-Carlo (uncertainty range 130%) $Q\alpha$ responses

These results show that the adaptive controller not only can prevent the loss of vehicle in several cases but also slightly improves the performance of the baseline controller. It is recognized that a more aggressive adaptive control tuning might improve these metrics, but that would generate a more intrusive adaptive controller strategy, causing more impact on the nominal performance of the baseline controller. Furthermore, it is noticeable that the LPV design shows an overall superior performance with respect to the baseline and adaptive controllers. In particular, it is highlighted that the LPV controller achieves a 30% reduction of the average $Q\alpha$ peaks.

V. Conclusions

This paper illustrates the design of an adaptive controller for the VEGA launcher based on NASA's SLS adaptive augmenting control algorithm. This design relies on a structured $\mathcal{H}_\infty$ baseline controller, which is augmented by the adaptive augmentation to extend safety envelope capabilities and increase performance under extreme off-nominal conditions.

In this article, the adaptive design is compared with the baseline controller (without adaptation) and a LPV design. Unlike the adaptive controller, which has been tuned empirically using nonlinear simulations, the baseline and LPV controllers were designed within a robust control framework, which provides a more systematic design methodology and also offers more analysis and design capabilities.

The three controllers are analysed using a set of nonlinear test cases with different uncertainty configurations and also via a Monte-Carlo campaign using an extended uncertainty range. The results show that the adaptive augmentation control law can successfully prevent severe failures such as loss of vehicle and slightly improve the performance of the baseline controller under uncertainty levels beyond the mission range. Nevertheless, the LPV controller is also capable of preventing such failures while improving performance and robustness with respect the adaptive scheme. Furthermore, this is achieved using a more methodological synthesis approach versus the tuning complexity of the adaptive law and the lack of adaptive analysis tools.

Acknowledgments

This work is funded by the European Space Agency (ESA) through the Networking/Partnering Initiative contract No. 4000114460/15/NL/MH/ats. Mr. Diego Navarro-Tapia is also the recipient of a Doctoral Training Partnership award No. 1609551 by the UK Engineering and Physical Sciences Research Council (EPSRC).

References

[1]Roux, C. and Cruciani, I., "Scheduling Schems and Control Law Robustness in Atmospheric Flight of VEGA," *Proceedings of the International ESA Conference on Guidance, Navigation and Control Systems*, 2008.

[2]Navarro-Tapia, D., Marcos, A., Bennani, S., and Roux, C., "Structured H-infinity Control Design for the VEGA Launch Vehicle: Recovery of the Legacy Control Behaviour," *Proceedings of the* 10^{th} *International ESA Conference on Guidance, Navigation and Control Systems (ESA-GNC)*, May 2017.

[3]Navarro-Tapia, D., Marcos, A., Bennani, S., and Roux, C., "Joint Robust Structured $\mathcal{H}_\infty$ Design of VEGA Launcher's Rigid-body Controller and Bending Filter," *Proceedings of the* 69^{th} *International Astronautical Congress (IAC)*, oct 2018.

[4]Navarro-Tapia, D., Marcos, A., Bennani, S., and Roux, C., "Linear Parameter Varying Control Synthesis for the Atmospheric Phase VEGA Launcher," *Proceedings of the* 2^{nd} *IFAC Workshop on Linear Parameter Varying Systems (LPVS)*, sep 2018.

[5]Simplício, P., Bennani, S., Marcos, A., Roux, C., and Lefort, X., "Structured Singular-Value Analysis of the Vega Launcher in Atmospheric Flight," *Journal of Guidance, Control, and Dynamics*, Vol. 39, No. 6, 2016, pp. 1342 – 1355.

[6]Orr, J. S., Wall, J. H., VanZwieten, T. S., and Hall, C. E., *Space Launch System Ascent Flight Control System*, NASA AAS 14-038, 2014.

[7]Orr, J. S. and s. VanZwieten, T., "Robust, Practical Adaptive Control for Launch Vehicles," *AIAA Guidance, Navigation, and Control Conference*, American Institute of Aeronautics and Astronautics, aug 2012.

[8]Wall, J. H., Orr, J. S., and VanZwieten, T. S., *Space Launch System Implementation of Adaptive Augmenting Control*, NASA AAS 14-051, 2014.

[9]VanZwieten, T. S., Gilligan, E. T., and Wall, J. H., *Adaptive Augmenting Control Flight Characterization Experiment on an F/A-18*, NASA AAS 17-126, 2017.

[10]Hodel, A., Whorton, M., and Jim Zhu, J., "Stability Metrics for Simulation and Flight-Software Assessment and Monitoring of Adaptive Control Assist Compensators," *Proceedings of AIAA Guidance, Navigation, and Control Conference*, aug 2008.

[11]Clements, K. and Wall, J. H., *Time Domain Stability Margin Assessment of the NASA Space Launch System GN%C Design for Exploration Mission One*, NASA AAS 17-126, 2017.

[12]VanZwieten, T. S., Hannan, M. R., and Wall, J. H., "Evaluating the Stability of NASA's Space Launch System with Adaptive Augmenting Control," *Proceedings of the* 10^{th} *International ESA Conference on Guidance, Navigation and Control Systems (ESA-GNC)*, May 2017.

[13]Arianespace, "VEGA Flight VV05," 2015, http://www.arianespace.com/mission/vega-flight-vv05/.

[14]Marcos, A., Rosa, P., Roux, C., Bartolini, M., and Bennani, S., "An overview of the RFCS project V&V framework: optimization-based and linear tools for worst-case search," *CEAS Space Journal*, Vol. 7, No. 2, 2015, pp. 303–318.

[15]Apkarian, P., Noll, D., and Rondepierre, A., "Mixed H2/Hinf Control via Nonsmooth Optimization," *Proceedings of the* 48^{th} *IEEE Conference on Decision and Control (CDC) held jointly with the* 28^{th} *Chinese Control Conference*, December 2009.

[16]Gahinet, P. and Apkarian, P., "Structured $\mathcal{H}_\infty$ Synthesis in MATLAB," *Proceedings of the* 18^{th} *World Congress of the International Federation of Automatic Control (IFAC)*, Vol. 18, August 2011, pp. 1435–1440.

[17]Hjartarson, A., Seiler, P., and Packard, A., "LPVTools: A Toolbox for Modeling, Analysis, and Synthesis of Parameter Varying Control Systems," *IFAC-PapersOnLine*, Vol. 48, No. 26, 2015, pp. 139 – 145.